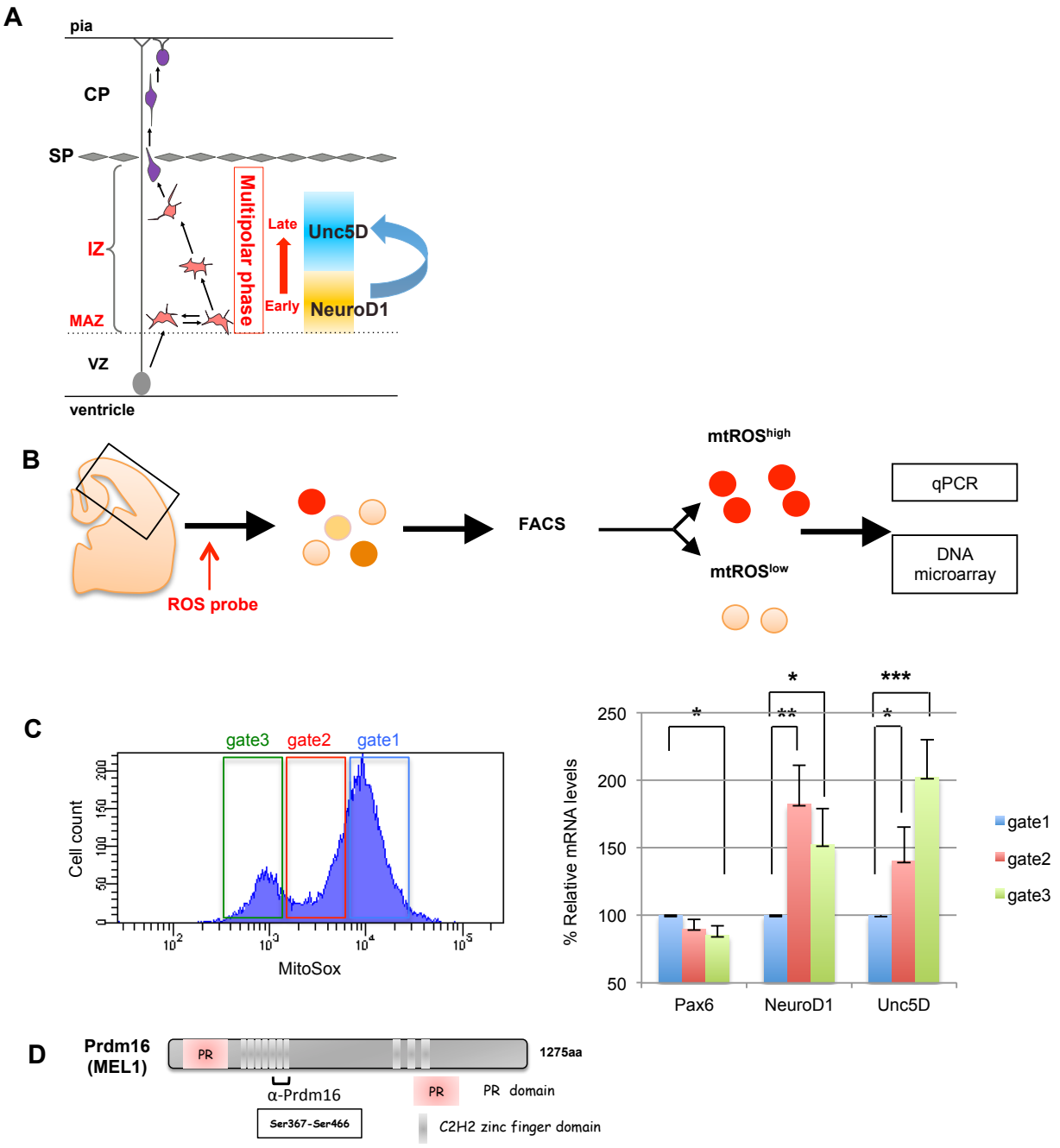

Figure S1. Progression of the postmitotic multipolar cell phase coordinates with changes in gene expression, and the changes in mtROS levels during differentiation were closely correlated with differentiation levels. (A) Schematic illustration of the sequential expression of NeuroD1 and Unc5D that coincide with early postmitotic differentiation in neocortical development (Inoue et al., 2014; Miyoshi and Fishell, 2012). (B) Schematic illustration of the experimental method for Figure 2C and D to isolate cell populations with different mtROS levels. (C) Dissociated cells were segregated into three populations according to mtROS levels and expression profiling among three sorted populations was performed using qPCR analysis. *p < 0.01, **p < 0.001, ***p < 0.0001; independent experiments from different littermates (n = 5). (D) Anti-Prdm16 antibody was generated to characterize its expression.

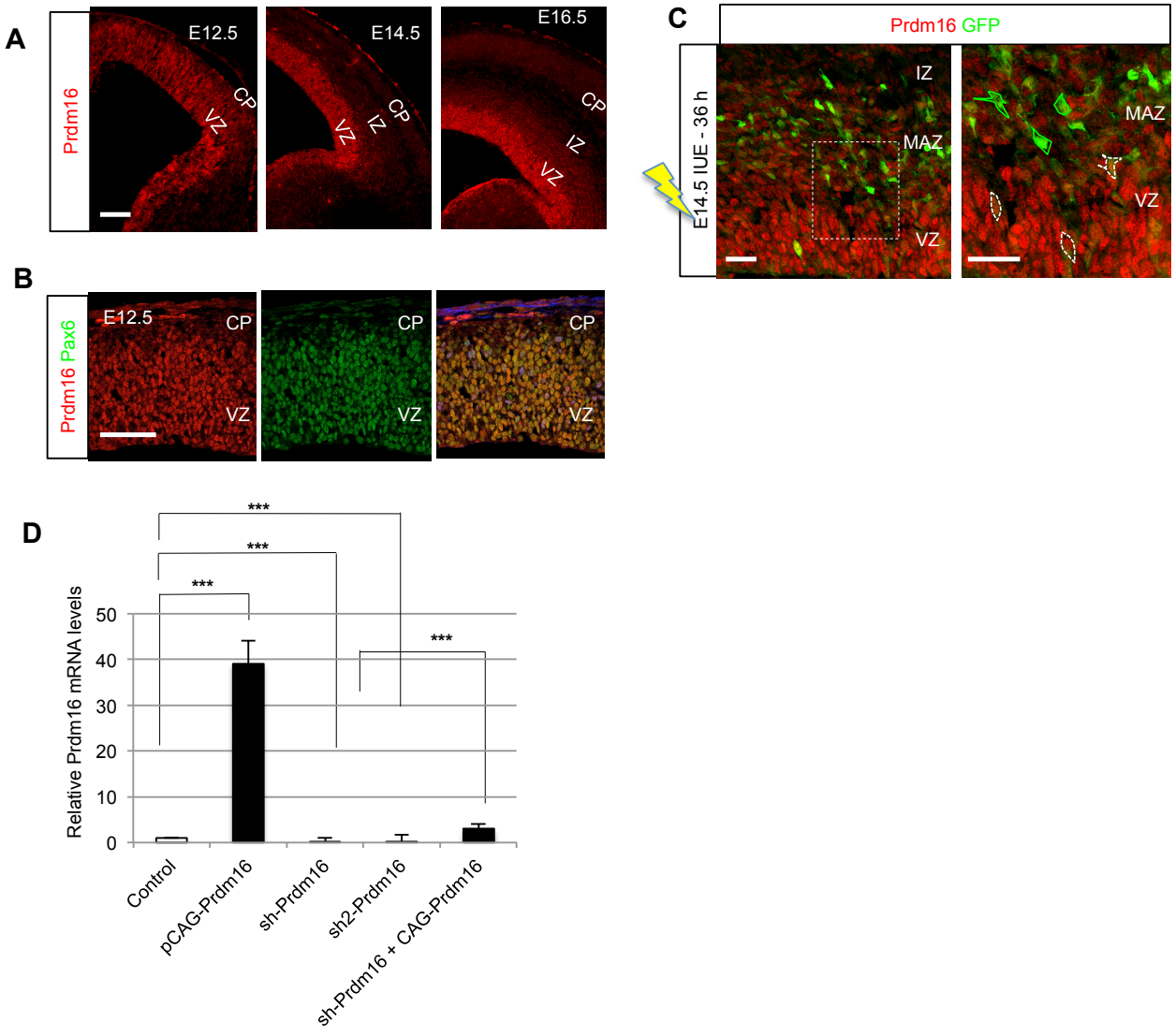

Figure S2. Prdm16 is preferentially expressed in VZ. (A and B) Immunostaining data show that Prdm16 was strongly expressed in the VZ of developing neocortex. Scale bar, 100 μm. (C) To recognize MAZ just above VZ, IUE of CAG-EGFP was introduced at E14.5 and analyzed 36 h later in accordance with a previous study (Tabata et al., 2012). Scale bar, 50 μm. (D) Both overexpression or knockdown vector for Prdm16 was transfected into primary culture, and confirmed Prdm16 mRNA levels; ***p < 0.01; independent experiments (n = 5).

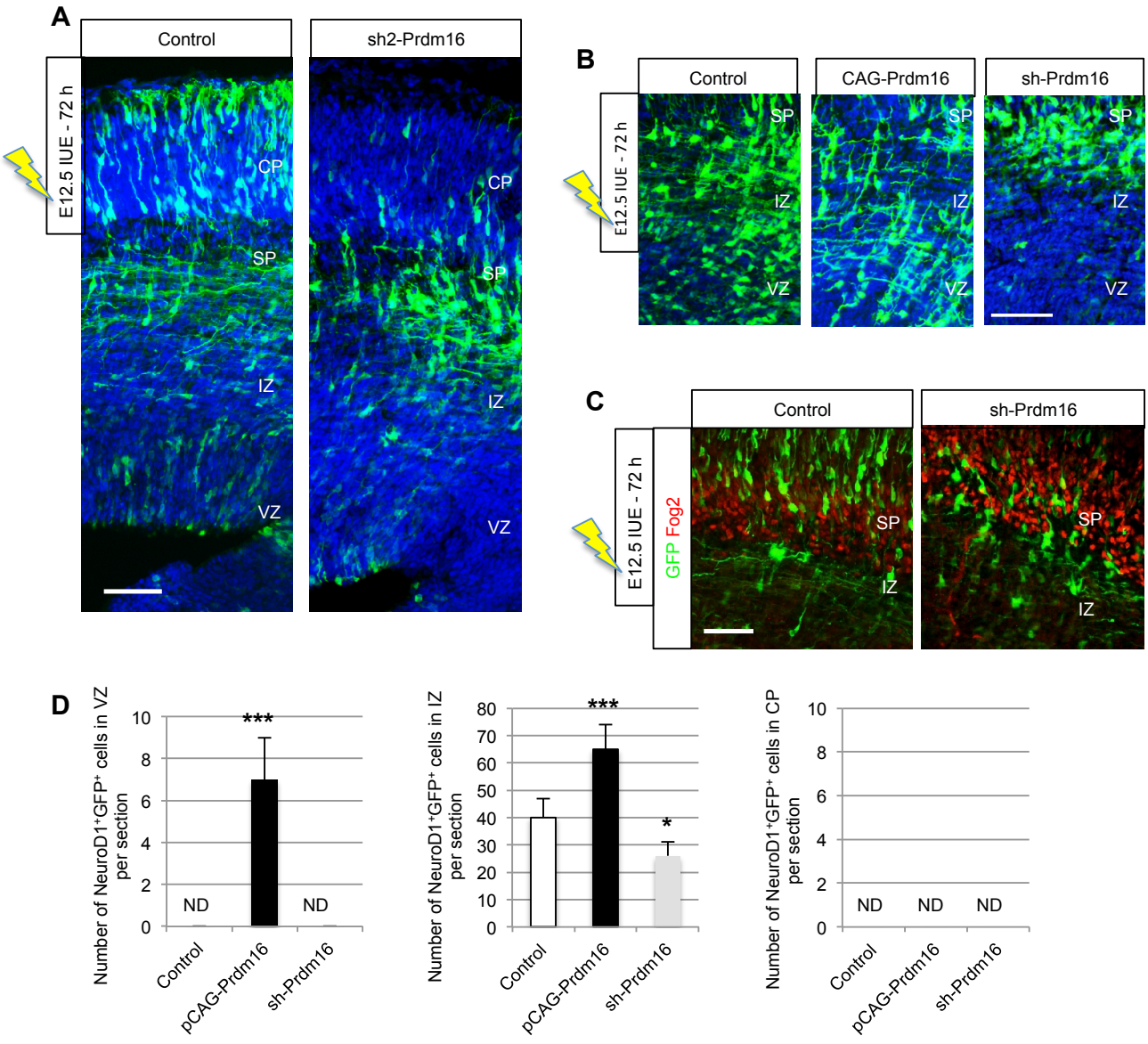

Figure S3. Prdm16 is required for appropriate development of multipolar cells.
(A) IUE of control and another Prdm16 LOF vector (sh2-Prdm16) was performed at E12.5, and brains were then analyzed 72 h after electroporation; Scale bar, 100 μm. (B) High-power images from Figure 4C; Scale bar, 100 μm. (C) Knockdown cells could not normally migrate or invade into SP, an area positive for Fog2, after IUE of the Prdm16 LOF vector at E14.5. Scale bar, 50 μm. (D) Co-IUE of sh-Prdm16 or CAG-Prdm16 in the presence of NeuroD1p-mCherry plasmids at E13.5 which were analyzed 36 h later. The cortex was divided into VZ, IZ, and CP, and the number of EGFP-positive NeuroD1-positive cells was quantified. *p < 0.01, ***p < 0.0001, ND: not detected; (n = 8 slices from eight individual brains).

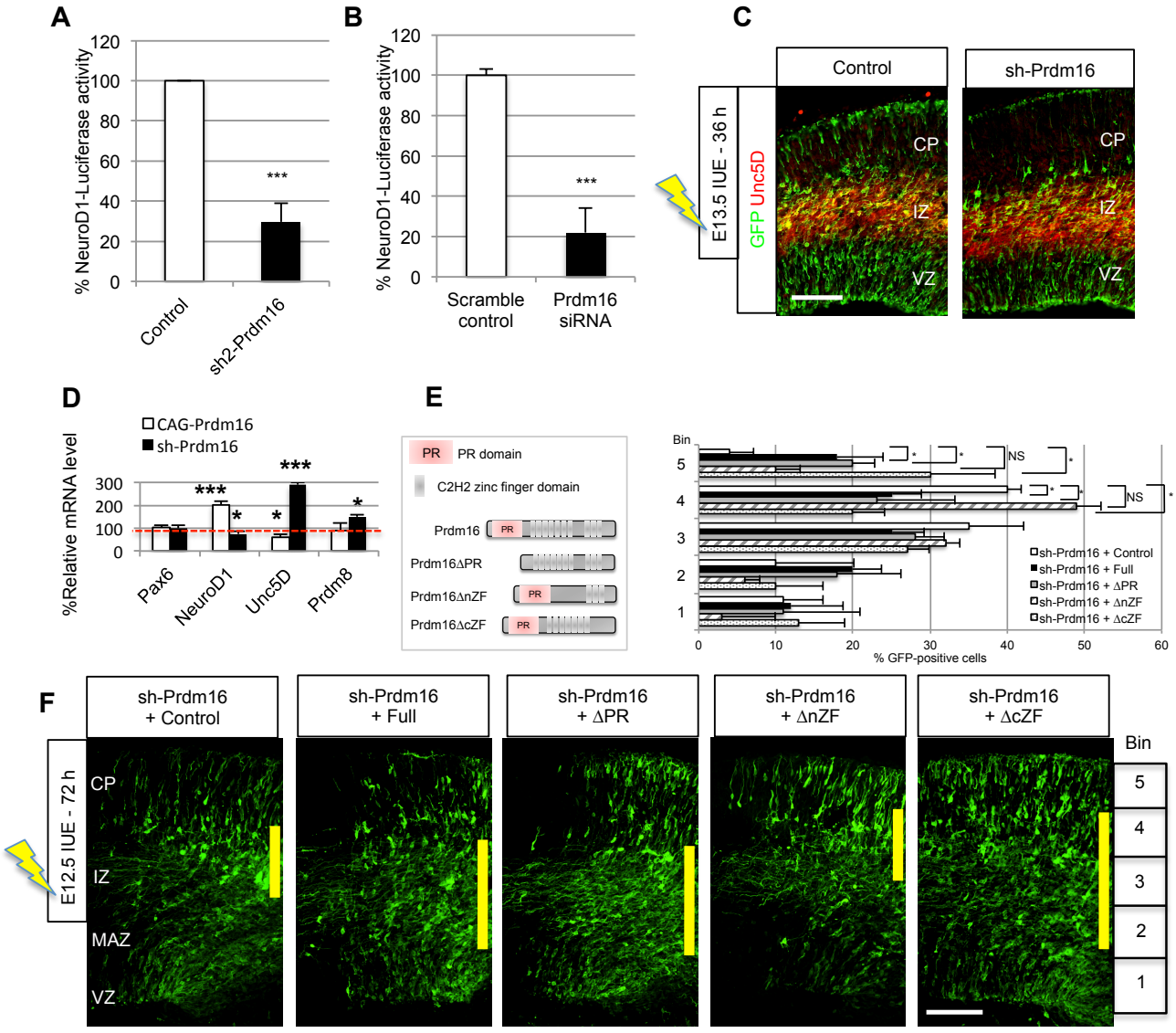

Figure S4. Prdm16 lacking nZF could not rescue migration defects induced by Prdm16 LOF.
(A and B) Reporter constructs were designed to express firefly luciferase in response to NeuroD1 and were transfected into Neuro2a cells in the presence of (A) sh2-Prdm16 or (B) Prdm16 siRNA; ***p < 0.0001; independent experiments (n = 5). (C) IUE of the control, Prdm16 GOF, or Prdm16 LOF vectors was performed at E13.5, and the brains were analyzed 36 h after electroporation. Furthermore, immunostaining with GFP and Unc5D was performed (n = 16 slices from eight individual brains). Scale bar, 100 µm. (D) qPCR analysis of marker genes in EGFP-sorted primary neural progenitor cultures after the co-transfection of CAG-EGFP and Prdm16 overexpression or knockdown vectors. *p < 0.01, ***p < 0.0001; independent experiments (n = 8). (E) Schematic illustration of a deletion mutant of Prdm16 expression vectors that lacks PR or ZF domain. (F) Co-IUE of sh-Prdm16 and CAG-Prdm16 expression plasmids or mutant plasmids ΔPR, ΔnZF, or ΔcZF at E12.5 which were analyzed 72 h later. The cortex was divided into five bins, and the proportion of EGFP-positive cells was quantified. *p < 0.01, NS: not significant; independent sections (n = 10) from five individual brains. Scale bar, 100 µm.

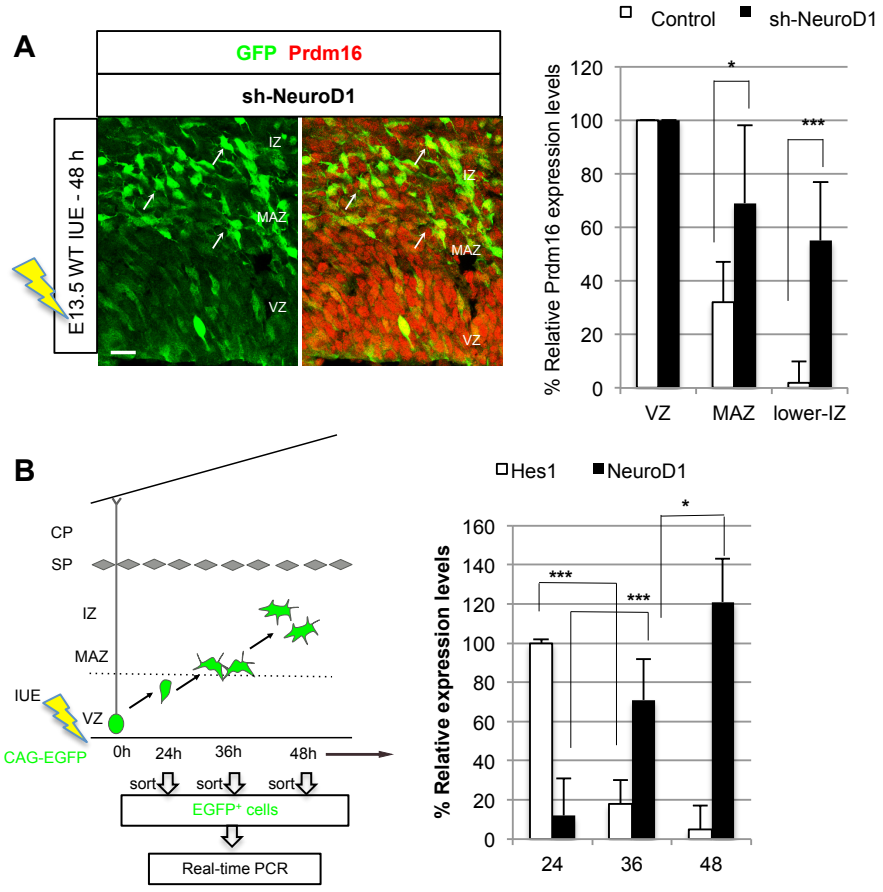

Figure S5. Prdm16 expression is negatively regulated by NeuroD1.

(A) IUE of control or NeuroD1-knockdown plasmids was performed at E13.5 and was analyzed after 48 h. Immunostaining with Prdm16 (red) was then performed to compare expression levels of Prdm16 between control and sh-NeuroD1 transfected cells. Boundaries between the VZ, the MAZ, and the IZ were deduced from orientations and densities of nuclei (Kelava 2012, Tabata 2009), and Prdm16 expression levels at each position were quantified. Cellular fluorescence intensities were analyzed using MetaMorph software and black levels were kept constant for each measurement. The pixel intensity threshold for red was adjusted so that the tissue background corresponded to level 0. About 200 randomly-selected GFP+ cells in the VZ, the MAZ, and the IZ were quantified; n = 4 slices from four individuals. Scale bar, 10 μm. *p < 0.01, ***p < 0.0001. (B) Schematic illustration of the experimental method for Figures 5F and S5B; GFP+ cell populations were isolated according to dissociation time points after IUE. Embryonic brains were harvested at 24, 36, and 48 h after the IUE of control GFP on E14.5, GFP-positive cells were sorted using FACS, and Hes1 and NeuroD1 mRNA levels were determined using qPCR. Sorted GFP+ cells were mainly from the VZ at 24 h after IUE, were mainly from the MAZ after 36 h IUE, and were mainly from the IZ after 48 h IUE, as shown previously (Tabata, 2009). To test whether NeuroD1 exerts feedback regulation against Prdm16 at specific time points (Figure 5F), GFP and sh-NeuroD1 were cotransfected with GFP plasmids on E14.5 and GFP-positive cells were sorted using FACS, and Prdm16 mRNA expression was determined (Figure 5F) at each time point. *p < 0.01, ***p < 0.0001

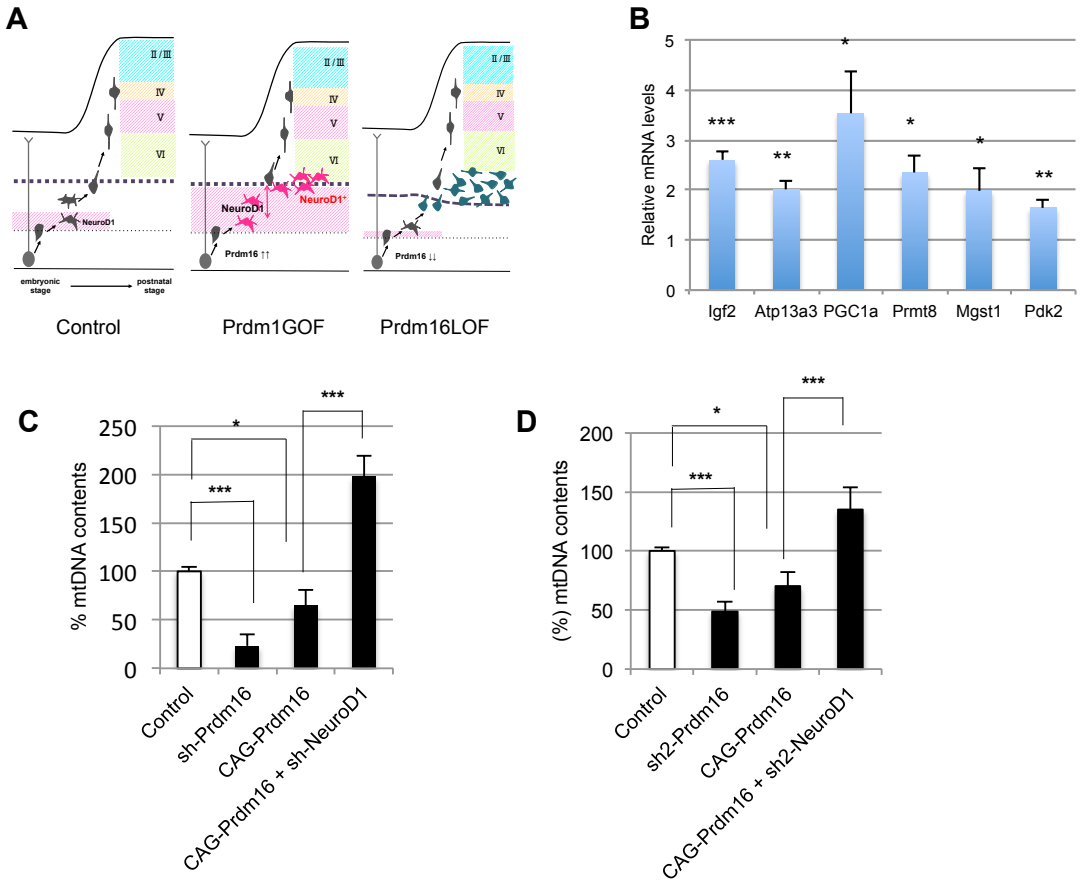

Figure S6. Co-transfection of sh-NeuroD1 with Prdm16 GOF vectors increased mtDNA contents . (A) A schematic illustration summarizes the role of Prdm16 in the control of temporal NeuroD1 expression, correlated with appropriate layer formation in the neocortex. (B) qPCR analysis of EGFP-sorted primary neural progenitor cultures after the co-transfection of CAG-EGFP and Prdm16 overexpression vectors. *p < 0.01, **p < 0.001, ***p < 0.0001; independent experiments (n = 5). (C and D) Relative mtDNA contents were determined in neocortical primary cultures transfected with (C) sh-Prdm16 or (D) sh2-Prdm16, CAG-Prdm16 in the presence or absence of (C) sh-NeuroD1 or (D) sh2-NeuroD1 ; *p < 0.01, ***p < 0.0001; independent experiments (n = 3).

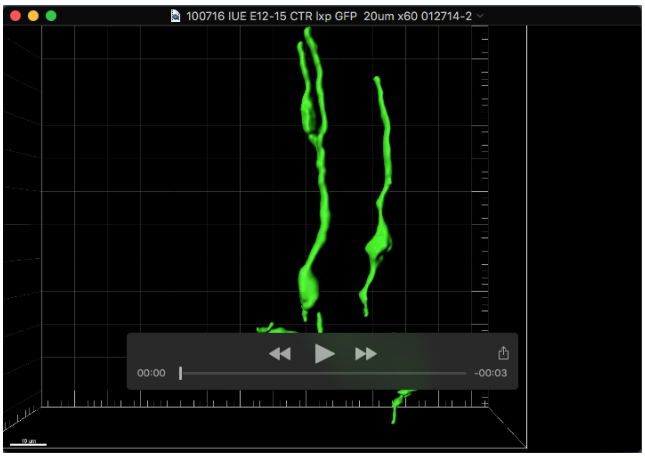

Movie 1. Clonal labeling of typical morphology of multipolar and bipolar cells in the vicinity of the SP with a Cre-loxP expression plasmid system in the presence of control plasmid. Immunofluorescence of GFP in neocortical sections at 48 h after IUE; Z-stack confocal images around the SP were reconstructed using Imaris.

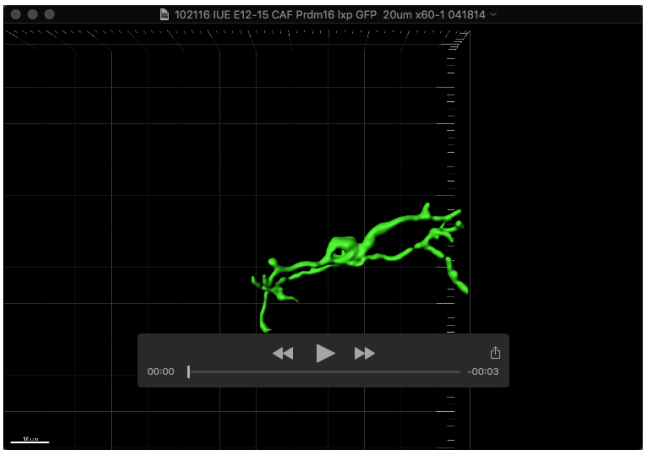

Movie 2. Clonal labeling of typical morphology of multipolar cells in the vicinity of the SP with a Cre-loxP expression plasmid system in the presence of Prdm16GOF plasmid. Immunofluorescence of GFP in neocortical sections at 48 h after IUE; Z-stack confocal images around the SP were reconstructed using Imaris.

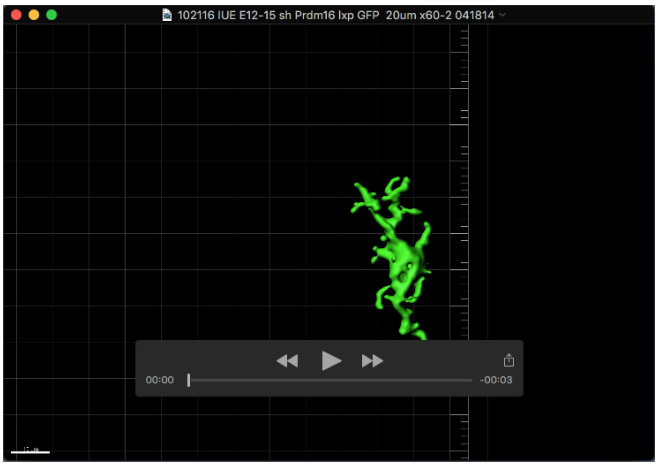

Movie 3. Clonal labeling of typical morphology of aberrant cells in the vicinity of the SP with a Cre-loxP expression plasmid system in the presence of Prdm16LOF plasmid. Immunofluorescence of GFP in neocortical sections at 48 h after IUE; Z-stack confocal images around the SP were reconstructed using Imaris.

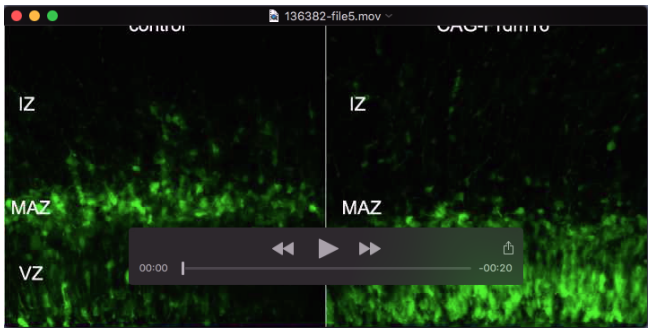

Movie 4. Prdm16-GOF cells show characteristic irregular migration in VZ, MAZ, and IZ.

IUE of control (left) or CAG-Prdm16 (right) was performed at E14.5. Cortical slices were prepared after 42 h and cultured under observation with a FV1000 confocal laser microscope. Time-lapse imaging data were then acquired automatically every 15 min for 28 h.

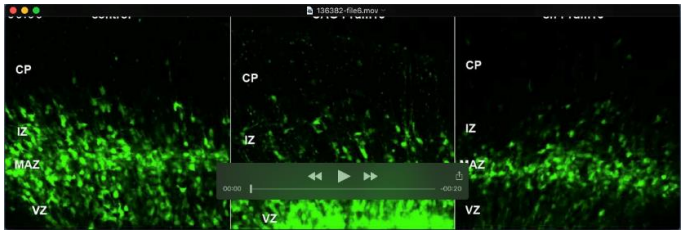

Movie 5. Prdm16-GOF cells show characteristic irregular migration, leading to the inhibition of CP invasion.

IUE of control, CAG-Prdm16 or sh-Prdm16 was performed at E13.5. Cortical slices were prepared after 36 h and cultured under observation with a FV1000 confocal laser microscope. Time-lapse imaging data were then acquired automatically every 15 min for 29 h.

SUPPLEMENTARY MATERIALS AND METHODS

Gain- and loss-of-function experiments

The knockdown efficiency of psh-Prdm16 and overexpression efficiency of pCAG-Prdm16 in the primary neural progenitors were confirmed by immunostaining (data not shown) and qPCR (supplementary material Fig. S2D). Rescue of the sh-Prdm16 phenotype was hampered by inappropriate Prdm16 levels for normal development. Thus, a second independent shRNA (sh2-Prdm16) was utilized to confirm the phenotype. Moreover, to confirm that knockdown effects of sh-Prdm16 and sh2-Prdm16 were specific to Prdm16 expression, we confirmed the absence of a phenotype relating to expression levels of the Prdm family transcription factor Prdm12 and Prdm5 (data not shown), and knockdown effect by psh-Prdm16 was rescued by the introduction of pCAG-Prdm16

(supplementary material Fig. S2D). The stealth RNAi for Prdm16 and its scrambled control (Thermo Fisher) were transfected with NeuroD1p-luciferase construct, and reproducibility of knockdown effect by sh-Prdm16 was confirmed (supplementary material Fig. S4B). The downregulation of Prdm16 expression by Prdm16-siRNA *in vivo* using IUE was also crucial for appropriate progression of the multipolar phase (data not shown).

Immunohistochemistry

Cryostat sections (20 μm) were treated with blocking buffer (10% donkey serum and 0.1% TritonX-100, pH 7.4) for 60 min at room temperature, followed by incubation with primary antibodies diluted (supplementary material Table S1) in the same buffer overnight at 4 degree. Sections were washed three times in 0.1% TritonX-100 (PBST) for 30 min and incubated 1 h at room temperature with secondary antibodies. The sections were washed three times in PBST for 30 min and incubated for 1 h at room temperature. After being washed, the sections were embedded on a cover glass with mounting medium (Prolong Gold, Invitrogen). For mouse anti-Prdm16 monoclonal antibody (Z1312) generation, cDNA fragments corresponding to the residues S367–S466 of mouse Prdm16 were subcloned into pBAC-surf1 (Merck Biosciences). The antibody specificity was confirmed by immunostaining against the Prdm16 knockout mouse brain, which was kindly provided by Dr. A. Moore (data not shown). EdU labeling *in vivo* (intraperitoneal injection of 12.5 mg/kg EdU) and staining were performed using the Click-IT EdU Imaging kit (Life Technologies) according to the manufacturer's instructions.

Microscopy and imaging analysis

We labeled multipolar cells with a Cre-loxP clonal expression plasmid system, pCAG-FloxP-EGFP-N1, and pCAG-Cre in the presence of a control, Prdm16 overexpression, or Prdm16 knockdown vector using IUE to more clearly monitor the morphological differences and counted the number of multipolar cells. Results are shown as mean ± SEM, and Student's t-test was used. n = 3 experiments brains coming from at least 3 different experiments. All images were acquired and quantified while blinded to the transfected plasmids.

Furthermore, we used IUE to more closely examine the multipolar cells. It has previously been reported that EGFP-positive cells that express NeuroD1 during the emergence of multipolar cells just above VZ, in an area called MAZ, are typically observed 36 h after IUE at E14.5 (Tabata et al., 2009, 2012, 2013). Therefore, we identified EGFP-positive cells after 36 h of IUE in MAZ, separated them into three groups positioned below SP (VZ, MAZ, and IZ), and compared the Prdm16 expression levels. For quantification, the intensity of fluorescent excitation of cells, gain and black levels were kept constant for each session of measurement, and fluorescent intensity in each cell was measured using Olympus IX81 powered by the MetaMorph analysis software. Mean data of approximately 200 cells in each region was calculated as Prdm16 expression levels for MAZ or IZ and expressed as percentage of VZ. n = 3 experiments brains coming from at least 3 different experiments.

Quantitative real-time PCR

Total RNA was isolated using RNeasy Mini Kit (Qiagen) according to the manufacturer's instruction. cDNA was synthesized from 1 μg of RNA using QuantiTect Retrotranscriptase reaction (Qiagen). qPCR was performed using SYBR green labeling (SYBR Premix Ex

TaqII, Takara) and a TP850 Real-Time PCR System (Takara). The primers used were listed in supplementary material Table S2. GAPDH expression was used to normalize the samples, and each sample was run in triplicate. mtDNA was quantified using qPCR with primers shown in supplementary material Table S2. The relative mtDNA copy number was calculated from the ratio of mtDNA copies to nuclear DNA (nucDNA) copies (Puente et al., 2014). The relative fold change was then calculated based on the ΔΔCt method.

DNA microarray analysis

Total RNA was prepared using a RNeasy Mini kit (Qiagen), and the quality was assessed with a BioPhotometer plus (Eppendorf). cDNA synthesis and cRNA-labeling reactions were performed using the 3′IVT-Express Kit according to manufacturer's instructions (Affymetrix). High-density oligonucleotide arrays for Mus musculus (Mouse Genome 430 2.0) containing 39,000 probes were performed according to the Expression Analysis Technical Manual (Affymetrix).

Cell sorting from electroporated brains

We harvested the embryonic brains at 24 h, 36 h, and 48 h after the IUE of control GFP on E14.5, sorted GFP-positive cells using FACS, and determined Hes1 and NeuroD1 mRNA level using qPCR. We confirmed that sorted GFP-positive cells at 24 h after the IUE contained mainly VZ cells, at 36 h contained mainly MAZ cells, and at 48 h contained mainly MAZ cells (Figure S5B); this was consistent with the results of a previous study (Tabata et al., 2009). Therefore, the same technique was utilized to compare mtDNA content during differentiation (Figure 1F) among VZ cells, MAZ cells, and IZ cells.

In addition, to test whether NeuroD1 exerts feedback regulation against Prdm16 at specific time points, GFP-positive cell populations were isolated according to dissociation time points after IUE. Schematic illustration of the experimental method was shown in Figures 5F. Embryonic brains were harvested at 24, 36, and 48 h after the IUE of control GFP on E14.5, GFP-positive cells were sorted using FACS, and Prdm16 mRNA expression was determined (Figure 5F) at each time point. n = 3 experiments brains coming from at least 3 different experiments.

Luciferase assay

Luciferase reporter assay was performed using E14.5 primary neocortical culture or Neuro2a cells. After transient transfection, cells were cultured for 24 h. Cell lysates were made using Dual-Luciferase Assay System (Promega), and luciferase activity of each lysate was measured in triplicate by a luminometer (GloMax®-Multi Detection System, Promega). Firefly luciferase activity was normalized relative to the activity of Renilla luciferase. The luciferase constructs for Hes1, Ngn2, NeuroD1, and PGC1α were kindly provided by Drs. H. Shimojo and A. Fukamizu, respectively.

Time-lapse imaging

Approximately 10-20 optical Z sections were acquired automatically every 15 min for about 30 h, and 20 focal planes (50 μm thick) were merged to visualize the entire shape of the cells. Representative migration trajectories of neurons observed in the control, GOF, and LOF experiments were traced using MTrackJ (a plugin for ImageJ software, NIH). The migration speed was calculated by dividing the migration distance achieved by each cell

by the duration of tracking. Statistical analyses shown in Figure 6C was performed using Student's t-test (Statcel 3, OMC Inc.). To analyze the migration speed in Figure 6F, the trajectories of migrating neurons were automatically traced by using TrackMate plugin (ImageJ software, NIH). The data of each group (control, GFP and LOF) were obtained from 4~6 brains in 2 independent experiments (> 600 cells/group), and the differences were assessed by one-way ANOVA and Tukey-Kramer post hoc test (Statcel 3, OMC Inc.).

Table S1. Antibodies list

Antibody	Supplier	Cat No.	Dilution
Goat anti-Brn2	Santa Cruz	sc-6029	1:100
Goat anti-NeuroD1	Santa Cruz	sc-1084	1:100
Goat anti-Unc5D	R&D systems	AF1429	1:100
Rabbit anti-DsRed	TaKaRa	632496	1:500
Rabbit anti-Fog2	Santa Cruz	sc-10755	1:50
Rabbit anti-GFP	Torrey Pines Biolabs	TP401	1:200
Rabbit anti-Sox5	GenWay	18-003-42358	1:200
Rabbit anti-Tbr2	abcam	ab23345	1:300
Rat anti-GFP	nacalai tesque	04404-26	1:500
PE mouse anti-CD133	eBioscience	12-1331-82	1:1000
Donkey secondary antibodies conjugated to Alexa fluorophores A488, A594, A647	Invitrogen		1:500

Table S2. Primer Sequences used in real-time PCR

Gene	Species	Forward Primer	Reverse Primer
Atp13a3	mouse	GAATGGGGGAGGAGCAGT	ATCCAATTCCAGCCACCA
GAPDH	mouse	AGCTTGTCATCAACGGGAAG	TTTGATGTTAGTGGGGTCTCG
Hes1	mouse	AAAGCCTATCATGGAGAAGAGGCG	GGAATGCCGGGAGCTATCTTTCTT
Igf2	mouse	AAAGCCATCTCCCCGTTC	ACTGGGATCCCCATTGGT
Mgst1	mouse	ACCTCAGGCAGCTCATGG	TGGCATTCTCTCCCTTGC
mtDNA	mouse	CCCATTCCACTTCTGATTACC	ATGATAGTAGAGTTGAGTAGCG
NeuroD1	mouse	CTCAGCATCAATGGCAACTTCTC	GACTCGCTCATGATGCGAATGCC
Ngn2	mouse	TAGGATGTTCGTCAAATCTGAGAC	CGCGCTGGAGGACATC
nucDNA	mouse	GTACCCACCTGTCGTCC	GTCCACGAGACCAATGACTG
Pax6	mouse	CCAGCATGCAGAACAGTCAC	CATCTGCATGGGTCTGCAG
Pdk2	mouse	AAAGACCCCGAGGACCAC	TGGTGCTGCCATCAAAGA
PGC1a	mouse	GAAAGGGCCAAACAGAGAGA	GTAAATCACACGGCGCTCTT
Prdm16	mouse	AGGGCAAGAACCATTACACG	AGAGGTGGTCGTGGGTACAG
Prmt8	mouse	TGCCAGGGACAAGTGGTT	TTGCTTTGGGTCCACGAT
Unc5D	mouse	CACCAGGGCTGACCATAAC	TCCATTCACGTAGACCACC